Effects of Casimir force on high-order sideband generation in an optomechanical system

Jie Yao (姚 洁), Yafei Yu (於亚飞)*, and Zhiming Zhang (张智明)**

Guangdong Provincial Key Laboratory of Nanophotonic Functional Materials and Devices (School of Information and Optoelectronic Science and Engineering); Guangdong Provincial Key Laboratory of Quantum Engineering and Quantum Materials, South China Normal University, Guangzhou 510006, China

**Corresponding author: yfyuks@hotmail.com; **corresponding author: zmzhang@scnu.edu.cn*

Received August 9, 2018; accepted September 29, 2018; posted online October 31, 2018

We introduce a Casimir force in a conventional optomechanical system to study the high-order sideband generation. In this system, a nanosphere is placed near the moveable mirror of the conventional optomechanical system. The moveable mirror is coupled to the cavity field and the nanosphere by the optomechanical interaction and the Casimir interaction, respectively. We find that the amplitude and cutoff order of the high-order sideband can be enhanced by decreasing the sphere–mirror separation (increasing the Casimir force) and increasing the optomechanical coupling strength. Our proposal provides an alternative method for generating the high-order sidebands and for measuring the Casimir force.

OCIS codes: 120.4880, 270.0270.
doi: 10.3788/COL201816.111201.

Cavity optomechanics[1,2] is a rapidly growing field that explores the interaction between light and mechanical motion via radiation pressure force. It has many potential applications in quantum information processing[3,4], quantum communication[5], optical storage[6], detection of gravitational waves[7,8], and so on. Because cavity optomechanics can relate the classical physics and quantum physics, it has aroused extensive interest and intensive research. Many important effects in optomechanical systems have been observed, such as optomechanically induced transparency[9–12], electromagnetically induced transparency[13], quantum squeezing[14,15], and optomechanically induced nonreciprocity[16,17]. Moreover, many nonperturbative phenomena have also been revealed based on the optomechanical interaction, such as Akhmediev breathers[18]. However, when we consider the nonlinear terms in the evolution equations, some other phenomena will appear, such as high-order sideband generation[19–22] and optomechanically induced sum (difference)-sideband generation[23,24].

Casimir force[25–27] is an attractive force between uncharged metallic surfaces caused by the vacuum fluctuations. Recently, the high-precision measurement of Casimir force was carried out by many groups[28,29]. In particular, Mohideen and Roy performed a precision measurement of Casimir force between a metallic sphere and a flat plate using an atomic force microscope. Casimir force can generate and affect a series of phenomena that arise from the interaction between mechanical and cavity modes, such as optomechanical entanglement[30]. Nie *et al.* discussed the dynamics of a hybrid optomechanical setup, where a dielectric nanosphere is levitated inside the Fabry–Perot cavity of a standard optomechanical system and is coupled to the cavity field and the movable mirror by the optomechanical and Casimir interactions[31]. Liu *et al.* studied the optomechanically induced transparency with a tunable Casimir force[32].

In this Letter, we theoretically investigate the effect of Casimir force on the high-order sideband generation in an optomechanical system, in which a nanosphere is placed near the moveable mirror of the standard optomechanical system. The nanosphere is coupled to the moveable mirror by Casimir force. We find that the amplitude and cutoff order of the high-order sideband can be enhanced by decreasing the sphere–mirror separation and increasing the optomechanical coupling strength.

Our model is shown in Fig. 1, in which a gold-coated nanosphere is coupled to the oscillating mirror of a standard optomechanical system via the Casimir force. The system is driven by two fields: a controlling field with frequency ω_l and a probe field with frequency ω_p. The Hamiltonian of the system can be written as[32]

$$\begin{aligned} H = {} & \hbar\omega_c \hat{a}^\dagger \hat{a} + \left(\frac{\hat{p}^2}{2m} + \frac{1}{2} m\omega_m^2 \hat{x}^2\right) \\ & - \hbar g \hat{a}^\dagger \hat{a}\, \hat{x} - \frac{\pi^3 \hbar c R}{720(d-\hat{x})^2} + i\hbar\varepsilon_l (\hat{a}^\dagger e^{-i\omega_l t} - \text{H.c}) \\ & + i\hbar(\varepsilon_p \hat{a}^\dagger e^{-i\omega_p t} - \text{H.c}), \end{aligned} \tag{1}$$

where the first term is the free Hamiltonian of the cavity field, in which $\hat{a}(\hat{a}^\dagger)$ is the annihilation (creation) operator of the cavity field with frequency ω_c. The second term is the free Hamiltonian of the mechanical resonator with effective mass m and angular frequency ω_m, where $\hat{p}$ and $\hat{x}$ are the momentum and position operators of the mechanical resonator. The third term represents the interaction Hamiltonian between the cavity field and the movable mirror via the radiation pressure with the coupling strength $g = \omega_c/L$ (L is the cavity length). The fourth

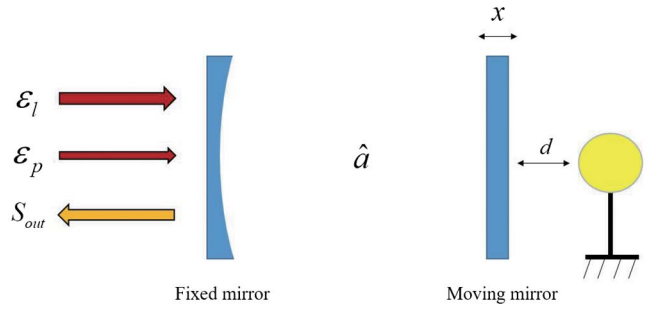

Fig. 1. Sketch of the system.

term denotes the interaction between the movable mirror and the nearby gold-coated nanosphere via the Casimir force, where R is the radius of the nanosphere, d represents the sphere–mirror separation, and c is the speed of light in vacuum. It should be noted that the distance between the nanosphere and the mechanical oscillator should be much smaller than the size of adjacent plane[32]. The last two terms describe the interactions of the cavity field with the controlling field and the probe field, respectively, with the amplitudes $\varepsilon_l = \sqrt{2\kappa P_l/\hbar\omega_l}$ and $\varepsilon_p = \sqrt{2\kappa P_p/\hbar\omega_p}$, where κ is the decay rate of the cavity field, P_l and P_p are the powers of the controlling field and the probe field, respectively.

In the rotating frame at the frequency ω_l, the Hamiltonian of Eq. (1) is given in the form as

$$\begin{aligned} H_{\rm rot} &= \hbar\Delta_l \hat{a}^\dagger \hat{a} + \left(\frac{\hat{p}^2}{2m} + \frac{1}{2} m\omega_m^2 \hat{x}^2\right) \\ &\quad - \hbar g \hat{a}^\dagger \hat{a}\, \hat{x} - \frac{\pi^3 \hbar c R}{720(d-\hat{x})^2} + i\hbar\varepsilon_l(\hat{a}^\dagger - \text{H.c}) \\ &\quad + i\hbar(\varepsilon_p \hat{a}^\dagger e^{-i\delta t} - \text{H.c}), \end{aligned} \tag{2}$$

where $\Delta_l = \omega_c - \omega_l$ and $\delta = \omega_p - \omega_l$ are the detunings of the cavity field and probe field from the controlling field, respectively.

Substituting the Hamiltonian into Heisenberg equations of motion and introducing the corresponding damping terms phenomenologically, we obtain

$$\begin{aligned} \dot{\hat{p}} &= -m\omega_m^2 \hat{x} + \hbar g \hat{a}^\dagger \hat{a} + \frac{2\pi^3 \hbar c R}{720(d-\hat{x})^3} - \Gamma_m \hat{p} + \hat{F}_{\rm th}, \\ \dot{\hat{x}} &= \frac{\hat{p}}{m}, \\ \dot{\hat{a}} &= -(i\Delta_l + \kappa - ig\hat{x})\hat{a} + \varepsilon_l + \varepsilon_p e^{-i\delta t} + \sqrt{2\kappa}\hat{a}_{\rm in}, \end{aligned} \tag{3}$$

where κ and Γ_m are the decay rates of cavity field and mechanical resonator, respectively. $\hat{F}_{\rm th}$ is the thermal noise, resulting from the coupling between the mirror and environment and satisfying $\langle \hat{F}_{\rm th}(t)\rangle = 0$[33]. The quantum noise of the cavity field is represented by $\hat{a}_{\rm in}$ with $\langle \hat{a}_{\rm in}(t)\rangle = 0$[33]. The operators can be reduced to their expectation values because we are only interested in the mean response of our system. By using the mean-field assumption $\langle \hat{a}\,\hat{b}\rangle = \langle \hat{a}\rangle\langle \hat{b}\rangle = ab$ and dropping the quantum and thermal noise terms (their expectation values are zero), we can write the evolution equations of the expectation values as

$$\begin{aligned} \dot{p} &= -m\omega_m^2 x + \hbar g a^* a + \frac{2\pi^3 \hbar c R}{720(d-x)^3} - \Gamma_m p, \\ \dot{x} &= \frac{p}{m}, \\ \dot{a} &= -(i\Delta_l + \kappa - igx)a + \varepsilon_l + \varepsilon_p e^{-i\delta t}. \end{aligned} \tag{4}$$

The steady-state solutions of Eq. (4) can be obtained as

$$\begin{aligned} a_s &= \frac{\varepsilon_l}{(i\Delta_l + \kappa) - igx_s}, x_s \\ &= \frac{1}{m\omega_m^2}\left[\hbar g |a_s|^2 + \frac{2\pi^3 \hbar c R}{720(d-x_s)^3}\right]. \end{aligned} \tag{5}$$

By using Eq. (5), we plot Fig. 2(a) and Fig. 2(b) to show the variation of the intracavity steady-state mean photon number $|a_s|^2$ with the sphere–mirror separation d and the power P_l of the controlling field. It can be seen from Fig. 2(a) that the steady-state mean photon number $|a_s|^2$ decreases with the increasing sphere–mirror separation and approaches a limit value when d is large enough. The reason for this is that the Casimir force decreases with the increase of d, and the limit value corresponds to the fact that the Casimir force can be neglected when d is large enough. Figure 2(b) shows that the intracavity steady-state mean photon number linearly increases with the power of the control field, and apparently, this is a reasonable result.

Now, we study the output spectrum of the system. The output spectrum is defined as[19,20]

$$S_{\rm out}(\omega) \propto \left| \int_{-\infty}^{+\infty} S_{\rm out}(t) e^{-i\omega t} {\rm d}t \right|, \tag{6}$$

in which $S_{\rm out}(t) = S_{\rm in}(t) - \sqrt{2\kappa}a(t)$ (the input–output relation), $S_{\rm in}(t) = \varepsilon_l e^{-i\omega_l t} + \varepsilon_p e^{-i\omega_p t}$, and $a(t)$ can be

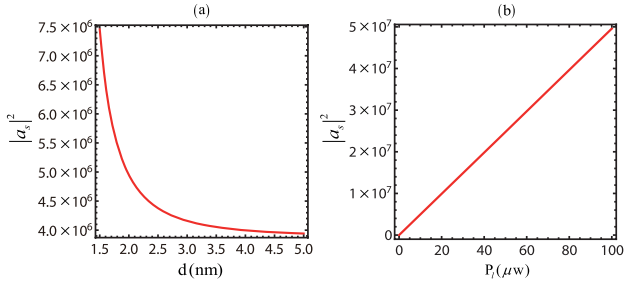

Fig. 2. Intracavity steady-state mean photon number $|a_s|^2$ varies with (a) the sphere–mirror separation and (b) the power of the controlling field. The parameters used are $m = 145$ ng, $\omega_m = 2\pi \times 947$ kHz, $\Gamma_m = 2\pi \times 141$ Hz, $R = 150$ nm, $\kappa = 2\pi \times 215$ Hz, $\omega_l = 2\,\pi c/\lambda$, $\lambda = 1064$ nm, $g = 2\pi \times 70$ GHz/μm, and $\Delta_l = \omega_m$. In addition, (a) $P_l = 10$ μW and (b) $d = 2$ nm.

obtained by solving the set of equations of Eq. (4). Since these equations are nonlinear, it is difficult to obtain analytical solutions, so we use the Runge–Kutta method to solve these equations with the initial conditions: $a|_{t=0} = 0, x|_{t=0} = 0, p|_{t=0} = 0$[34]. Before discussing the output spectrum in detail, we would like to point out that the spectra have a shift of frequency ω_l, since Eq. (4) describes the evolution of the system in the rotating frame at frequency ω_l.

Figure 3 shows the output spectra for different values of the sphere–mirror separation. In Fig. 3(a), we set the sphere–mirror separation d to ∞ (without Casimir force). We can find that the cutoff order of the high-order sideband is four, and the higher the order is, the weaker its intensity is. This is a feature of the perturbation regime. Next, we shorten the sphere–mirror separation d to 2 nm. As shown in Fig. 3(b), compared with Fig. 3(a), the cutoff order of the high-order sideband increases to six. We continue to decrease the sphere–mirror separation d to 1.8 nm. From Fig. 3(c), we can clearly see that some nonperturbation features appear in the spectrum, such as, the intensity of the second-order sideband is almost as strong as the first-order sideband, which is obviously different from the perturbation feature in Fig. 3(b). Not only does the cutoff order of the high-order sideband increase to nine, but also the corresponding intensities of the high-order sidebands increase with respect to Fig. 3(b). When we further decrease the sphere–mirror separation d to 1.5 nm, some more obvious nonperturbation spectral structures appear, as shown in Fig. 3(d). The intensities of the higher-order sidebands are significantly enhanced, and the intensities of some higher-order sidebands even exceed the first-order sideband, which is the typical nonperturbation feature of the high-order sideband generation. In summary, Fig. 3 shows that the cutoff order and the amplitude of high-order sidebands can be significantly enhanced by decreasing the sphere–mirror separation (increasing the Casimir force). Comparing with other methods for the high-order sideband generation, introducing a Casimir force in a conventional optomechanical system provides an alternative method for the controlling of the high-order sideband generation.

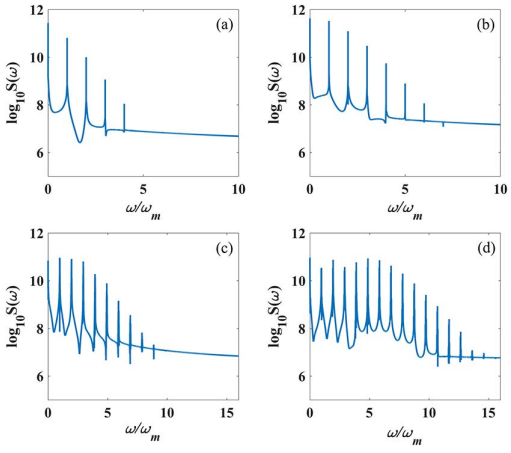

Fig. 3. Output spectra for different values of the sphere–mirror separation d: (a) $d = \infty$, (b) $d = 2$ nm, (c) $d = 1.8$ nm, and (d) $d = 1.5$ nm. We use $\varepsilon_p = \varepsilon_l/2$. The power of the controlling field is $P_l = 30$ μW. The other parameters are the same as in Fig. 2.

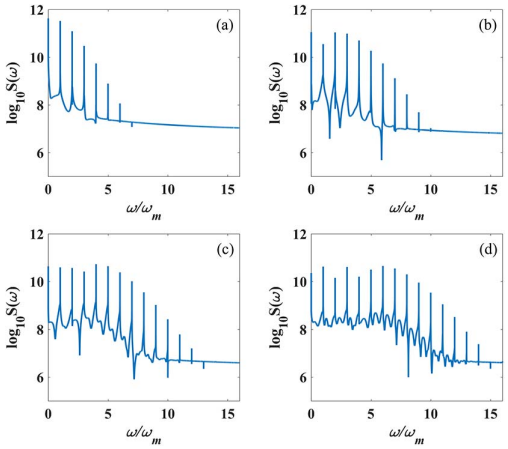

Fig. 4. Output spectra for different values of the optomechanical coupling strength g: (a) $g = g_0$, (b) $g = 2g_0$, (c) $g = 3g_0$, (d) $g = 4g_0$, here $g_0 = 70$ GHz/μm. The sphere–mirror separation is $d = 2$ nm. The other parameters are the same as in Fig. 2.

Figure 4 shows the output spectra for different values of the optomechanical coupling strength g. We can clearly see that both the cutoff order and the intensity of the high-order sidebands increase with increasing the coupling strength. Therefore, a stronger optomechanical coupling strength is more conducive to the generation of high-order sidebands.

In conclusion, we theoretically investigate the features of the high-order sideband generation in an optomechanical system controlled by a Casimir force. We find that the amplitude and cutoff order of the high-order sidebands can be enhanced with the decrease of the sphere–mirror separation (corresponding to the increase of the Casimir force). We also find that the amplitude and cutoff order of the high-order sidebands can be enhanced by increasing the optomechanical coupling strength. Our proposal provides an alternative method for the generation of the high-order sidebands and also a potential method for measuring the Casimir force. In current experiments, the distance for measuring the Casimir force is about 100 nm[35,36]. However, with the rapid advances of nano-fabrication techniques, a smaller distance can be expected in the near future[32].

This work was supported by the National Natural Science Foundation of China (Nos. 11574092, 61775062, 61378012, 91121023, and 60978009), the National Basic Research Program of China (No. 2013CB921804), and the Innovation Project of Graduate School of South China Normal University (No. 2017LKXM090).

References

1. T. J. Kippenberg and K. J. Vahala, Science **321**, 1172 (2008).
2. M. Aspelmeyer, T. J. Kippenberg, and F. Marquardt, Rev. Mod. Phys. **86**, 1391 (2014).

3. K. Stannigel, P. Komar, S. J. M. Habraken, S. D. Bennett, M. D. Lukin, P. Zoller, and P. Rabl, Phys. Rev. Lett. **109**, 013603 (2012).
4. P. Kómár, S. D. Bennett, K. Stannigel, S. J. M. Habraken, P. Rabl, P. Zoller, and M. D. Lukin, Phys. Rev. A **87**, 013839 (2013).
5. A. K. Ekert, Phys. Rev. Lett. **67**, 661 (1991).
6. V. Fiore, Y. Yang, M. C. Kuzyk, R. Barbour, L. Tian, and H. Wang, Phys. Rev. Lett. **107**, 133601 (2011).
7. L. Ju and D. G. Blair, Int. J. Mod. Phys. D **5**, 101 (1996).
8. D. D. Serafino, S. Gomez, L. Milano, F. Riccio, and G. Toraldo, J. Global Optim. **48**, 41 (2010).
9. S. Weis, S. Deléglise, R. Rivière, and E. Gavartin, Science **330**, 1520 (2010).
10. H. Xiong, L. G. Si, A. S. Zheng, X. Yang, and Y. Wu, Phys. Rev. A **86**, 013815 (2012).
11. P. C. Ma, J. Q. Zhang, Y. Xiao, M. Feng, and Z. M. Zhang, Phys. Rev. A **90**, 043825 (2014).
12. Y. Xiao, Y. F. Yu, and Z. M. Zhang, Opt. Express **22**, 17979 (2014).
13. Z. Q. Zhang, Z. H. Zhu, Z. H. Peng, C. L. Jiang, Y. F. Chai, and L. Tan, Chin. Opt. Lett. **16**, 012701 (2017).
14. A. Dalafi, M. H. Naderi, and A. Motazedifard, Phys. Rev. A **97**, 043619 (2018).
15. Q. H. Cai, Y. Xiao, Y. F. Yu, and Z. M. Zhang, Opt. Express **24**, 20036 (2016).
16. M. Hafezi and P. Rabl, Opt. Express **20**, 7672 (2011).
17. G. L. Li, X. Xiao, Y. Li, and X. G. Wang, Phys. Rev. A **97**, 023801 (2018).
18. H. Xiong and Y. Wu, Laser Photon. Rev. **12**, 1700305 (2018).
19. H. Xiong, L. G. Si, X. Y. Lü, X. X. Yang, and Y. Wu, Opt. Lett. **38**, 353 (2013).
20. L. G. Si, L. X. Guo, H. Xiong, and Y. Wu, Phys. Rev. A **97**, 023805 (2018).
21. Y. Jiao, H. Lü, J. Qian, Y. Li, and H. Jing, New J. Phys. **18**, 083034 (2016).
22. Z. X. Liu, H. Xiong, and Y. Wu, Phys. Rev. A **97**, 013801 (2018).
23. H. Xiong, L. G. Si, X. Y. Lü, and Y. Wu, Opt. Express **24**, 5773 (2016).
24. H. Xiong, Y. W. Fan, X. Yang, and Y. Wu, Appl. Phys. Lett. **109**, 061108 (2016).
25. H. B. G. Casimir, Proc. K. Ned. Akad. Wet. **51**, 793 (1948).
26. E. Elizalde and A. Romeo, Am. J. Phys. **59**, 711 (1991).
27. L. Spruch, Science **272**, 1452 (1996).
28. U. Mohideen and A. Roy, Phys. Rev. Lett. **81**, 4549 (1998).
29. J. L. Garrett, D. A. Somers, and J. N. Munday, Phys. Rev. Lett. **120**, 040401 (2018).
30. W. J. Nie, Y. H. Lan, Y. Li, and S. Y. Zhu, Phys. Rev. A **86**, 063809 (2012).
31. W. J. Nie, Y. H. Lan, Y. Li, and S. Y. Zhu, Phys. Rev. A **88**, 063849 (2013).
32. X. F. Liu, Y. Li, and H. Jing, Sci. Rep. **6**, 27102 (2016).
33. C. W. Gardiner and P. Zoller, *Quantum Noise* (Springer, 2004).
34. J. C. Butcher, *The Numerical Analysis of Ordinary Differential Equations: Runge–Kutta and General Linear Methods* (Wiley-Interscience, 1987).
35. H. B. Chan, Y. Bao, and J. Zou, Phys. Rev. Lett. **101**, 030401 (2008).
36. D. E. Krause, R. S. Decca, D. López, and E. Fischbach, Phys. Rev. Lett. **98**, 050403 (2007).